

BAR INSTABILITY IN DISK-HALO SYSTEMS

J. A. SELLWOOD

Department of Physics and Astronomy, Rutgers University, 136 Frelinghuysen Road, Piscataway, NJ 08854, USA
Revised version, submitted to ApJ, January 13, 2016

ABSTRACT

We show that the exponential growth rate of a bar in a stellar disk is substantially greater when the disk is embedded in a live halo than in a rigid one having the same mass distribution. We also find that the vigor of the instability in disk-halo systems varies with the shape of the halo velocity ellipsoid. Disks in rigid halos that are massive enough to be stable by the usual criteria, quickly form bars in isotropic halos and much greater halo mass is needed to avoid a strong bar; thus stability criteria derived for disks in rigid halos do not apply when the halo is responsive. The study presented here is of an idealized family of models with near uniform central rotation and that lack an extended halo; we present more realistic models with extended halos in a companion paper. The puzzle presented by the absence of strong bars in some galaxies having gently rising inner rotation curves is compounded by the results presented here.

Subject headings: galaxies: kinematics and dynamics – galaxies: spiral – galaxies: structure

1. INTRODUCTION

It has long been known that the dominant dynamical instability of massive stellar disks leads to the formation of a strong bar (Miller, Prendergast & Quirk 1970; Hohl 1971; Kalnajs 1972, 1977; Jalali 2007). The mode is an exponentiating standing wave between two reflection points: corotation where traveling waves are strongly amplified as they swing from leading to trailing (Goldreich & Lynden-Bell 1965; Julian & Toomre 1966), and the disk center where an ingoing trailing wave reflects into an outgoing leading wave. Toomre (1981), who elucidated this mechanism for the bar mode, also argued that the instability could be quelled in at least two ways. Toomre's preferred method was to interrupt feedback through the center, perhaps by ensuring that the waves are damped at an inner Lindblad resonance (ILR, Mark 1974), which should be present if the galaxy has a dense bulge, for example. This feature accounts for the remarkable linear stability of the Mestel, and other self-similar, disks (Zang 1976; Evans & Read 1998). High-quality simulations (Sellwood 1989; Sellwood & Moore 1999; Sellwood & Evans 2001) of massive disks having dense centers do indeed avoid bar-formation, as predicted by linear theory, but an ultra-responsive disk can amplify even a modest level of noise to such an extent that the linear theory expectation of damping at resonances can be overwhelmed, and particles become trapped into a bar through a non-linear instability. Thus, this stabilizing method may not always be effective, especially in a galaxy that experiences a strong perturbation. Random motions make the disk less responsive, and generally contribute to stability (*e.g.* Athanassoula & Sellwood 1986).

It is indeed true that the bar instability is quelled when the disk is immersed in a massive, unresponsive spheroidal component. The effect of the extra central attraction is to shorten the preferred wavelength of gravitationally-driven disturbances in the disk until bi-symmetric disturbances become no more than mild kinematic waves that can no longer extract much amplification from the global potential well of the galaxy

(Toomre 1981; Binney & Tremaine 2008). This is the basis of several well-known stability criteria (Ostriker & Peebles 1973; Efstathiou, Lake & Negroponte 1982; Christodoulou, Shlosman & Tohline 1995).

However, these criteria assume the halo is unresponsive, and here we show that a responsive halo encourages the bar instability in disks, and that these stability criteria are inadequate when the disk is immersed in a live halo. A hint of a more vigorous bar instability may have been present in the simulations reported by Athanassoula & Misiriotis (2002) and by Martinez-Valpuesta, Shlosman & Heller (2006), but the focus of those papers was on the surprising secular growth of the bars, which grew to encompass most of the disk. Here we find that, for models of isolated disk galaxies that do not have a high central density, the disk-halo system possesses an unstable bar-forming mode that remains quite vigorous unless the disk has very low mass or the velocity distribution of the halo is strongly radially biased.

In order to develop an understanding of the instability, we focus on the linear modes of highly idealized models of unstable disks that start out axisymmetric and form bars, which is clearly a situation that is unlikely to arise in nature. In addition, the halos of our models are not at all extended, a choice that enabled the use of anisotropic velocity distributions and also excluded the complications caused by secular bar growth. Berrier & Sellwood (2016) present slightly more realistic simulations having extended halos in which disk mass rises through slow infall and find that models lacking a central mass concentration continue to manifest similar behavior.

2. MODEL SET UP

We wish to create equilibrium, axisymmetric, disk-halo models with no bulge, in which the shape of the velocity ellipsoid of the halo particles can be varied.

2.1. Halo and disk

The requirement that the halo distribution function (DF) be anisotropic is particularly limiting, since many available methods to create equilibrium halos in the pres-

ence of a disk assume an isotropic halo DF. However, if we choose a spherical halo for which anisotropic DFs are known, we can use the adiabatic invariance of actions to determine the equilibrium DF of the halo after an additional mass component has built up, as originally set out by Young (1980). Sellwood & McGaugh (2005) gave a full description of the method for halo compression and showed that a spherical approximation is entirely adequate, even when the compressing component is a disk that is heavier than those used here. If the DF of the uncompressed model was originally a function of just two integrals, the DF of the compressed spherical halo remains a function of two actions: the radial action and total angular momentum.

We require a spherical model with known anisotropic DFs that also lacks a density cusp. From this very limited selection (Binney & Tremaine 2008), we have chosen the family of anisotropic models given by Dejonghe (1987) for the Plummer sphere, which has the density profile

$$\rho(r) = \frac{3M_P}{4\pi a^3} \left[1 + \left(\frac{r}{a} \right)^2 \right]^{-5/2}. \quad (1)$$

This mass distribution has a harmonic core, consistent with the gently rising rotation curves in late-type galaxies of lower luminosity (*e.g.* Carignan & Freeman 1985; Catinella, Giovanelli & Haynes 2006; de Blok *et al.* 2008). Since the density declines as r^{-5} when $r \gg a$, where a is the core radius, the function could not represent an extended halo. However, the models allow us to study the linear stability of a disk embedded in a live spherical component whose velocity anisotropy can be varied. It clearly cannot capture secular angular momentum exchanges between bars and extensive halos (Weinberg 1985; Debattista & Sellwood 2000); this behavior is included in experiments described in a later paper (Berrier & Sellwood 2016).

Dejonghe (1987) gives expressions (in terms of hypergeometric functions) for the DF, characterized by a parameter q that is related to the usual anisotropy parameter (Binney & Tremaine 2008) as:

$$\beta \equiv 1 - \frac{\sigma_\phi^2}{\sigma_r^2} = 1 - \frac{\sigma_\theta^2}{\sigma_r^2} = \frac{qr^2}{2(a^2 + r^2)}. \quad (2)$$

The DF is positive or zero for all bound values of the specific energy, E , and allowed specific total angular momentum, L , when $-\infty < q \leq 2$. These halos, which have no net angular momentum, are isotropic when $q = 0$, radially biased when $q > 0$ and tangentially biased when $q < 0$, with $q = -\infty$ giving a sphere composed of entirely circular orbits. All models with finite q become isotropic as $r/a \rightarrow 0$; anisotropy increases rapidly outwards and is already half its asymptotic value by $r = a$. The maximal radial bias is for $q = 2$, where $\beta \rightarrow 1$ for $r \gg a$. We use just three different halo DFs in this work: $q = 0$ (isotropic), $q = 2$ (maximal radial bias), and $q = -15$ (strong tangential bias).

Simulations of an isolated Plummer sphere with $q = 2$ revealed that it suffers from a radial orbit instability. The growth rate, $\sim 0.015(GM_P/a^3)^{1/2}$, was low but the outer halo became strongly prolate by $t \sim 300(a^3/GM_P)^{1/2}$ in a model with 10^6 particles. We continue to use initially spherical models that are compressed by the disk, and

allow them to evolve self-consistently.

When compressed by a disk, the spherical density profile is changed, of course, and Sellwood & McGaugh (2005) used this family of anisotropic models to illustrate how compressibility of a halo varied with radial bias, finding, as expected, that halo compression was reduced as radial pressure rises. The models in this paper have lower disk masses, however, and compression has a minor effect on the density and a negligible effect on the shape of the velocity ellipsoid.

We insert an exponential disk of surface density

$$\Sigma(R) = \frac{M_d}{2\pi R_d^2} e^{-R/R_d}. \quad (3)$$

We limit the extent of the disk by tapering the surface density with a function that varies as a cubic polynomial from unity at $R = 4.5R_d$ to zero at $R = 5R_d$. The disk has a Gaussian density profile in the vertical direction with $z_0 = 0.1R_d$.

This family of disk-halo models therefore has two further parameters, the ratio of halo to disk mass, M_P/M_d , and ratio of the disk scale length R_d to the halo core radius a . We have experimented with halo masses in the range $1 \leq M_P/M_d \leq 5$ and keep $a = 1.5R_d$ for the reason given below.

2.2. Initial velocities

To make the halo finite, we adopt a maximum energy of halo particles equal to the potential in the disk plane at $r = 8a$ and select halo particles with energies less than this from the compressed halo DF in the manner described by Debattista & Sellwood (2000, Appendix A). The rapid density decline when $r \gg a$ (eq. 1) implies that just a few percent of the total mass is eliminated by our energy bound, and the halo is in excellent equilibrium in the combined potential of the disk and halo.

We set the disk particles in orbital motion, add random speeds such that Toomre's $Q = 1.5$, and use the Jeans equations in the local approximation to set initial in-plane and vertical velocity balance for the disk particles in the numerically-computed gravitational field of the total mass distribution. As the disk mass generally contributes a moderate fraction at most of the central attraction, the Jeans equations yield a disk that is also in excellent initial equilibrium.

Figure 1 shows the rotation curves of five of our models with differing halo masses. The dotted curve shows the disk contribution computed from the finitely thick and tapered disk, which is the same for all cases. The shapes of the rotation curves are little affected by the mass of the halo, which was the reason for choosing $a = 1.5R_d$.

Sackett (1997) defined a maximum disk as one for which $(V_d/V_{\text{tot}})^2 \gtrsim 0.85$ at the radius at which the disk contribution peaks. The models shown in Fig. 1 are all therefore strongly submaximal since, at $R = 2R_d$, they have $(V_d/V_{\text{tot}})^2 = 0.476, 0.336, 0.264, 0.219,$ and 0.187 respectively for $M_P/M_d = 1, 2, 3, 4,$ and 5 .

The decrease of the circular speed at large radii is a consequence of our adopted Plummer halo. While some results in this study would probably be changed were a more extensive halo to be used, as we note in places, it seems likely that a supporting response to the linear instability that forms the initial bars (the principal result

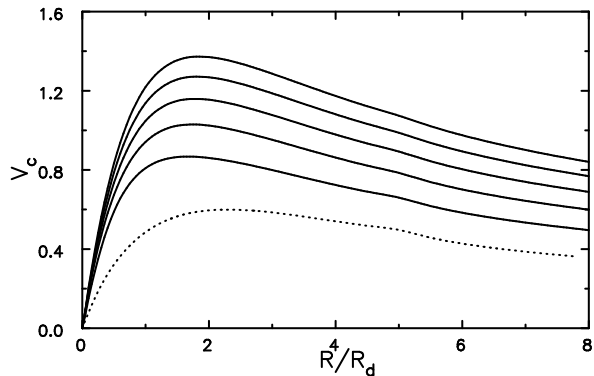


FIG. 1.— The radial variation of the circular speed in a series of models with differing halo masses. The unchanging disk contribution is shown by the dotted line, while the full drawn curves are for $M_P/M_d = 1, 2, 3, 4,$ and 5 .

presented below) would be provided by any reasonable live halo. In fact, the absence of an extended halo is an advantage, since it enables us to study the dynamical instability that forms the bar, without the complication of secular bar growth and braking caused by dynamical friction with an extended halo.

All the rotation curves rise nearly linearly from zero at the center, and this lack of shear in the inner parts is highly unfavorable for spiral arm development by swing amplification, as Sellwood & Carlberg (1984) reported. Thus our strongly submaximal models in rigid halos do not manifest multi-arm spirals of the kind found in other simulations of submaximal disks with more general rotation curve shapes (*e.g.* Fujii *et al.* 2011; Grand, Kawata & Cropper 2012).

Henceforth, we adopt M_d as our unit of mass, R_d , as our unit of length and set $G = 1$. Consequently, a dynamical time is $(R_d^3/GM_d)^{1/2}$ and the velocity unit is $(GM_d/R_d)^{1/2}$. Since we have smaller disk galaxies, such as M33, in mind, we suggest a scaling to physical units that sets $R_d = 1.4$ kpc (Regan & Vogel 1994) and $t_0 = 15$ Myr, which implies $M_d = 2.7 \times 10^9 M_\odot$ and velocities scale as $(GM/R_d)^{1/2} \simeq 91$ km/s. Thus the velocity rise to the peak shown in Fig. 1 roughly matches the inner rotation curve of M33 (Kam *et al.* 2015).

2.3. Numerical procedure

We use the hybrid N -body code described by Sellwood (2003, Appendix B), in which the gravitational field is computed with the aid of two grids: a 3D cylindrical polar grid for the disk component, and a spherical grid for the halo component with a surface harmonic expansion on each grid shell. A comprehensive description of our numerical methods is given in an on-line manual (Sellwood 2014).

We generally use 10^6 particles to represent each component, a time step $\delta t = 0.01$ dynamical times, include sectoral harmonics $0 \leq m \leq 8$ in the force determination on the cylindrical polar grid, where the cubic spline softening (Monaghan 1992) length is $0.2R_d$, and surface harmonics $0 \leq l \leq 4$ on the spherical grid. Aside from a time offset caused by a different seed amplitude, we found the evolution was unaffected when the numbers of disk and halo particles were varied over the range $10^5 \leq N \leq 10^7$, but $N = 10^4$ was clearly inadequate. We also verified

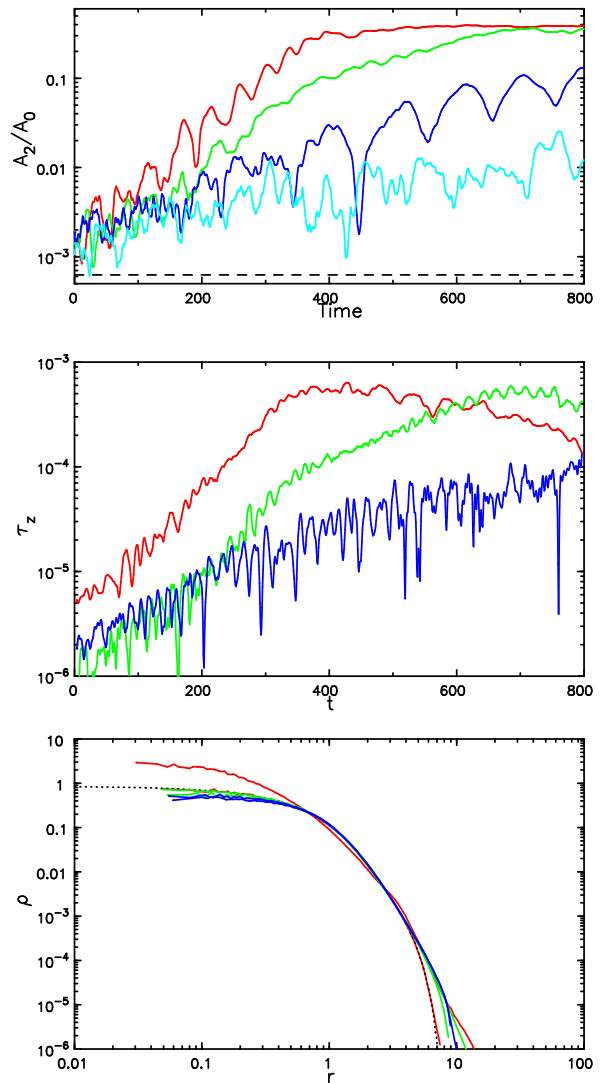


FIG. 2.— The evolution of four models with almost identical mass distributions, with $M_P/M_d = 3$, but having different DFs for the halo. The top panel shows the evolution of the bar amplitude in the disk component; the red curve is for a tangentially biased halo DF, the green for an isotropic halo, the blue for a radially biased halo DF, and the cyan for a rigid halo. The dashed horizontal line is the expected value of the ordinate if the particles were distributed at random in a axisymmetric disk. The middle panel shows the time evolution of the torque exerted by the disk on the live halo, colored as in the top panel. The bottom panel shows the initial and final halo density profiles for the three live halo models.

that moderate changes to the time step and grid size have little effect on the outcome of the simulations.

We recentered the grids on the particle centroid every 16 time steps, since an offset between the particle distribution and the center of our polar grids could lead to numerical artifacts. As a further check, we reran one case using a Cartesian grid, which has no preferred center and has adequate resolution for these models that do not have a high central density, and once again the evolution followed the same path.

3. BAR GROWTH

3.1. Halo anisotropy

The top panel in Figure 2 shows the evolution of the bar amplitude in the disk in four models having almost

identical mass distributions, but having different DFs for the halo. The quantity plotted is the ratio A_2/A_0 , where

$$A_m(t) = \left| \sum_j \mu_j e^{im\phi_j} \right|, \quad (4)$$

where μ_j is the mass and $\phi_j(t)$ the cylindrical polar angle of the j -th particle at time t , and the summation includes only disk particles. A straight line in this log-linear plot would be the signature of exponential growth; periodic modulations may indicate beats between two waves rotating with different pattern speeds.

The disk embedded in a rigid halo, cyan line, possesses very slowly growing, coherent bi-symmetric instabilities (see §4), causing the value of A_2/A_0 to rise slowly, by a factor ~ 10 over the duration of the simulation. However, the bar amplitude grows more rapidly in all three cases with live halos, and the behavior differs remarkably with the nature of the halo DF. The disk bar becomes strongest in the tangentially biased halo ($q = -15$, red curve), while slower bar growth occurs for the radially biased ($q = 2$, blue curve) halo DF. The isotropic halo ($q = 0$, green curve) is intermediate.

Notice that the value of A_2/A_0 reaches ~ 0.4 for the tangentially biased (red) and isotropic (green) models. These two bars become extremely strong inside $R \lesssim 3R_d$, where density variations from peak to trough are almost 100%. The value of $A_2/A_0 \gtrsim 0.1$ for the bar when the halo is radially biased halo (blue) is still visually discernible as an oval distortion to the inner disk by $t = 800$. This mass model should be comfortably stable in a rigid halo by conventional stability criteria: $t_{\text{OP}} = 0.10$ (Ostriker & Peebles 1973) and $V = 1.16(GM/R_d)^{1/2}$ at the peak of the rotation curve (Fig. 1 Efstathiou, Lake & Negroponte 1982). This prediction is indeed borne out by the cyan line in the top panel of Fig. 2 (see also §5.2), but the same model is clearly unstable when the halo is live whatever the shape of the halo velocity ellipsoid.

The middle panel shows the (smoothed) time evolution of the torque exerted by the disk on the halo, determined from the rate of gain of L_z by the halo, for the three cases with the live halo. Comparison of these curves with those in the top panel, reveals that the bar grows by giving angular momentum to the halo, since both the bar amplitude and the halo torque grow exponentially at approximately the same rate.

Note that the radially biased halo, which suffered from a radial orbit instability when isolated, seemed to remain closely spherical when the disk was inserted. Furthermore, since the bar grew more slowly, there is no evidence from the evolution of this model that a possible instability in the halo encourages the formation of a disk bar.

The loss of angular momentum from the disk causes the disk mass distribution to become more concentrated, which in turn causes additional compression of the halo, overwhelming any tendency for the halo to expand as a result of gaining angular momentum. Halo compression (bottom panel) is most pronounced for the tangentially biased DF, red curves, partly because more angular momentum is lost from the disk (middle panel) and partly because the lower radial pressure makes a tangentially biased halo more compressible. The smaller angular mo-

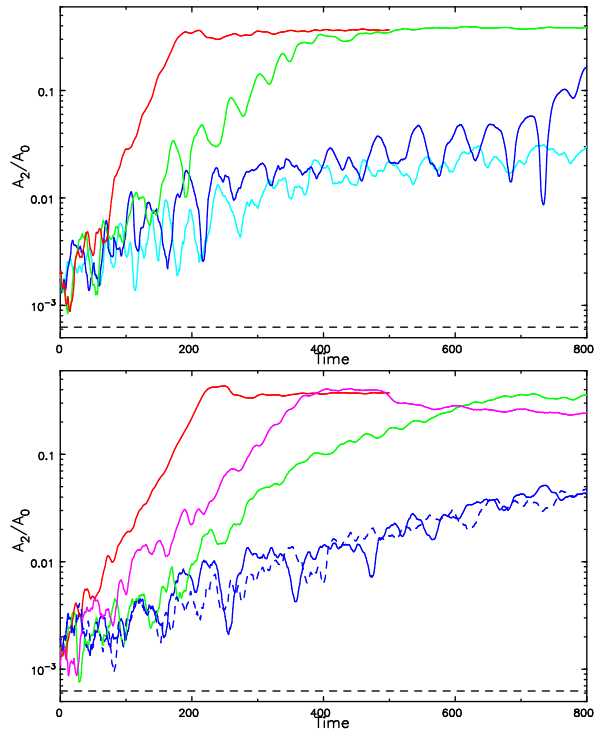


FIG. 3.— The time evolution of the bar amplitude in models with differing M_P/M_d . In the upper panel, all halos have tangentially biased DFs, while the halo DFs are isotropic in the lower panel. The value of M_P/M_d is denoted by the line color: red for $M_P/M_d = 2$, green for $M_P/M_d = 3$ (reproduced from Fig 2), blue for $M_P/M_d = 4$, and cyan for $M_P/M_d = 5$. The magenta line in the lower panel is for a rigid halo with $M_P/M_d = 2$, and the dashed blue line is from the same $M_P/M_d = 4$ model, but with the evolution computed on a Cartesian grid.

mentum changes and stiffer halos make the halo density changes in the other two models too small to notice.

3.2. Other halo masses

Figure 3 shows the consequence of changing the halo mass. The results in the upper panel are from simulations in which the halo velocity ellipsoid was strongly tangentially biased ($q = -15$), while it was isotropic in the lower panel. Since the disk in a rigid halo, even, has a vigorous bar instability when $M_P/M_d = 2$ (magenta line, lower panel), the rapid rise in the bar amplitude for the corresponding live halos, red lines, is hardly surprising, although it is noteworthy that the growth rates are clearly higher when the halo is live, and more so for the tangentially biased case.

However, the other curves for more massive halos continue to reveal bar growth on a time scale that slows both with increasing halo mass and with a shrinking fraction of near circular orbits in the halo. The green curves are from models with $M_P/M_d = 3$ that are simply reproduced from Fig. 2, but the blue curves and the cyan curve are from models with $M_P/M_d = 4$ and 5, respectively. While these models have lower growth rates, the instability is still clearly present.

3.3. Properties of the bars

Some bars in these disks become very strong, and buckle out of the plane, in the usual manner, to make peanut shapes that are very pronounced for the strongest

bars. The bars always form and remain fast, *i.e.* corotation is close to the end of the bar. The halo mass beyond the disk edge at $R = 5R_d$ in these simulations is less than 8% of the total in all the runs reported in this paper. The absence of an extended halo almost certainly inhibits bar slow-down through dynamical friction, and therefore these bars should not be regarded as counter-examples to the expectation (Debatista & Sellwood 2000) that $\mathcal{R} \equiv a_B/R_c \gtrsim 1.4$ for strong bars immersed in dense halos.¹ This aspect also prevented the kind of secular growth reported by Athanassoula & Misiriotis (2002) and Martinez-Valpuesta, Shlosman & Heller (2006), where the bars grew continuously to encompass the entire original disk.

4. LINEAR INSTABILITIES

4.1. Mode fitting

Although these are not “quiet start” simulations, the initial noise is low enough that the disturbances grow almost 100-fold before saturating, which affords reasonable estimates of the exponential growth rate. We used the mode fitting apparatus described in Sellwood & Athanassoula (1986) to estimate eigenfrequencies for the most rapidly growing modes over the period of linear growth. The Fourier coefficients of the density on the cylindrical polar grid, as well as logarithmic spiral transforms of the disk particles yield data that may be fitted with exponentially growing and rotating modes. The fitted mode generally has a complex frequency ω , where $\Re(\omega) = m\Omega_p$, with Ω_p being the pattern speed and $m = 2$ for bisymmetric modes, and $\Im(\omega)$ is the e -folding rate.

The crosses in Figure 4 show the best estimate of the growth rate of the most rapidly growing mode in each simulation, and the error bars indicate the spread in values from multiple fits to slightly different time ranges, fitted data type, rescaling factors, *etc.* More than a single mode seemed to be required to fit the data from some simulations, especially where the amplitude appears to be modulated. In these cases, the estimated pattern speeds of the two disturbances differ by about the right amount to account for the beat period, but a single, strong bar prevails in every case that reaches large amplitude.

Note that all the measured pattern speeds of all the growing modes reported here are high enough to avoid ILRs.

The case with the rigid halo with $M_P/M_d = 3$ (cyan curve, top panel of Fig. 2), possesses perhaps three very mildly growing coherent bisymmetric disturbances that we were able to identify in this long simulation. The shapes of these three waves show the classic pattern (Toomre 1981; Binney & Tremaine 2008) of interference between ingoing and outgoing waves, with more nodes for the lower frequency waves, as expected for a low mass disk in a rigid halo.

The behavior of the estimated growth rates in Fig. 4 with both halo mass and with the halo velocity distribution is consistent with the evolution of the amplitudes presented in Figs 2 and 3. At all halo masses, the cyan

¹ The dimensionless ratio $\mathcal{R} \equiv R_c/a_B$, originally defined by Elmegreen (1996), with R_c being the bar corotation radius and a_B being the semi-major axis of the bar, characterizes the bar angular speed.

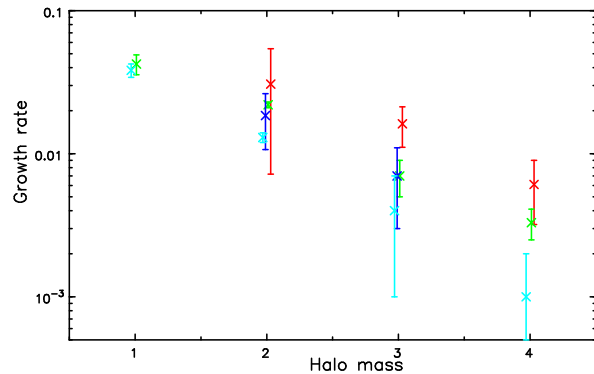


FIG. 4.— The estimated growth rates of the most unstable mode as a function of increasing halo mass. The colors signify the nature of the halo DF, as in Fig. 2; red for tangentially biased, green for isotropic, blue for radial bias, and cyan for a frozen halo. The halo mass is the same for each group of points, which are offset horizontally for clarity.

points indicate that disks in rigid halos have the lowest growth rates compared with those from live halos, whatever the form of the DF. Notice that the spread in growth rate at each halo mass broadens as the halo becomes more massive, implying that growth rates decline more slowly with increasing halo mass in live halos and most slowly in halos with tangentially biased DFs. Compared with that in the rigid halo, the bar growth rates range up to five times higher for the most massive responsive halo; even an isotropic DF causes the mode to have a three times higher growth rate.

4.2. Mode mechanism

Phase coherence and exponential growth indicate that the disturbances are dynamical instabilities of the disk-plus-halo system. Since the modes lack ILRs, the instability appears to have a similar feed-back mechanism to that of the bar instability of massive disks reviewed in the introduction, with the exception that amplification is boosted by interaction with the halo.

It is well-known (Lynden-Bell & Kalnajs 1972) that, when halo interactions are excluded, a disk inside corotation loses angular momentum, and that outside gains, as a self-excited mode grows. The outward transfer of angular momentum across corotation is accomplished by the spiral torque of the disturbance density. In our simulations with live halos, the torque from the disk on the halo (Fig. 2 middle panel) grows exponentially with the mode until it saturates, indicating that the bar is excited in these cases by the loss of angular momentum to the halo, and probably to the outer disk also. The substantial differences in the disk bar growth rate when the halo DF is changed, while keeping the halo density almost constant, is clear evidence that halo particles on near circular orbits couple most strongly to the density disturbance in the disk.

Increasing the halo mass slows the instability. The relative frequencies of disk and halo orbits must be little affected by changing halo mass, since both the disk and halo particles move in the same global potential. The more likely explanation is that the relatively less massive and more tightly wrapped disturbances in the disk couple less effectively to the more massive halos.

5. DISCUSSION

5.1. *Two obvious questions*

The results presented here are so startling, it is reasonable to ask two questions: (1) can they be right? and, if so, (2) why is the importance of responsive halos to the bar instability not more generally known?

We already reported in §2 that our results were insensitive to particle number, time step, grid resolution and even the type of grid, as shown by the solid and dashed blue lines in the lower panel of Fig. 3. Furthermore, Athanassoula & Misiriotis (2002) and Martínez-Valpuesta, Shlosman & Heller (2006), who both used direct- N methods, stressed the effect of the halo on the disk bar in their simulations of sub-maximal disks, but the bars in their models must have resulted from the same linear instability that we have identified. Thus there seems little room to doubt the numerical results reported here.

The well-cited papers by Athanassoula & Misiriotis (2002) and Martínez-Valpuesta, Shlosman & Heller (2006) reported just a couple of cases that may well have been unstable had they used rigid halos, yet the formation of bars in sub-maximal disks has not hitherto been followed up with a systematic study. In part, this could be because to use a tree code for this kind of study would require $\gtrsim 100$ times more computer time (Sellwood 2014) than the code we used here, which is able to compute the evolution of these models for a Hubble time with modest computational resources. Yet the more likely reason for no previous focused investigation may be that it is unfashionable to use simulations to study a single aspect of galaxy dynamics. Instead, many workers prefer to include all possible relevant complications, such as “gas-trophysics,” halo triaxiality, substructure, *etc.* into every simulation. While a strong case can be made for this approach, it comes with two clear disadvantages: it not only makes the simulations very costly in computer time, but it also renders the few results that can be obtained much more difficult to understand.

5.2. *Disk stability*

The difference of behavior between live and rigid halos is not qualitative, but simply that growth rates are higher. As has been reported before (*e.g.* Toomre 1981), disks in even very massive rigid halos continue to possess mild bisymmetric instabilities, even though they are believed to be “stable.”

Thus, the practical question of disk stability is perhaps best cast as whether a bar would grow by less than some large factor, one hundred or ~ 5 e -folds say, in a Hubble time or 800 dynamical times, which translates to $\Im(\omega) \lesssim 0.006$ in the units of this paper. By this criterion, disk stability requires a more massive live halo than a rigid one. Judging from the slopes of the growth rate measurements in Fig. 4, the halo need be some 30% – 50% more massive for the growth rate in a responsive isotropic halo to match that in a rigid halo.

Note that this conclusion is indicated by isotropic halos in this one mass model, and that a more general stability criterion, if one exists, would require an extensive study to explore many different mass models and halo DFs. Note also, that in models having a dense center, such as a bulge, the disk can be linearly stable at much higher mass

fraction than in these cases with gently rising rotation curves (Berrier & Sellwood 2016).

5.3. *Implications for real galaxies*

Higher growth rates for bar instabilities in live halos make the survival of unbarred disks in bulgeless galaxies, which already had no clear explanation (Sellwood 2013), still more perplexing. The growth rate can be suppressed by reducing the disk mass, or by making the halo DF strongly radially biased, or by raising the level of random motion in the disk. We discuss all these options in turn, finding each quite unattractive.

The usual argument against the rigid halo explanation for disk stability is that it predicts (Sellwood & Carlberg 1984; Athanassoula *et al.* 1987) that galaxy disks should be dominated by small-scale, multi-arm spirals, as found by others (*e.g.* Fujii *et al.* 2011; Grand, Kawata & Cropper 2012; D’Onghia, Vogelsberger & Hernquist 2013). We have shown here that live halos, unless they are strongly radially biased right to near the center, would require still lower disk masses. In further experiments, to be described later, we again observe tightly-wrapped, multi-arm spirals in cool disks in compressed, isotropic Einasto halos that are massive enough to suppress the bar. However, nature does not appear to prefer this solution, since observations (*e.g.* Davis *et al.* 2012), find that the majority of spiral patterns in galaxies have $m = 2$ or 3.

Relaxed halos from dark matter only Λ CDM simulations are mostly isotropic near their centers and become mildly radially biased by the virial radius, where $\beta \simeq 0.35$ (Diemand & Moore 2011). Very little seems to have been reported of how the velocity ellipsoid shape is affected by baryonic infall and feedback, but a dramatic change would seem unlikely. Thus there is no reason to expect a *strong* radial bias in the inner parts of the halos of real galaxies that would materially improve the stability of real galaxy disks.

Disks with large degrees of random motion will be more stable than cool disks (Athanassoula & Sellwood 1986). Current galaxy formation models (Governato *et al.* 2010; Scannapieco *et al.* 2012; Christensen *et al.* 2014) favor strong “feedback” from dense gas clumps that impulsively eject large gas masses from the disk after adiabatic infall. The effect of this repeated irreversible cycle is both to lower the halo density and to make the remaining stellar disk quite puffy with large random motions in all three components. While random motion among the disk stars must be stabilizing, the galaxies that present the greatest stability puzzles are late-type spirals with stellar masses in the range few $\times 10^8$ to several $\times 10^9 M_\odot$. These galaxies have little in the way of bulge light, which is why their rotation curves rise slowly in the inner parts (Catinella, Giovanelli & Haynes 2006), and lie in the mass range of greatest flattening (*e.g.* Sánchez-Janssen, Méndez-Abreu & Aguerri 2010). Furthermore, they usually have reasonably well-developed spiral patterns, which is another indicator that the disk cannot be so hot as to be dynamically unresponsive.

Thus, if galaxies are indeed embedded in responsive dark matter halos, then the fact that a significant fraction of them lack a strong bar is still more perplexing than before.

It is particularly puzzling that M33 supports a coher-

ent two-arm spiral pattern and at the same time has no more than a very weak bar (Regan & Vogel 1994). This is because a bi-symmetric spiral pattern suggests a massive disk; strong swing amplification is generally required either for a self-excited mode or for an amplified mild tidal perturbation. Since swing amplification at $m = 2$ is negligible in a low-mass disk (Toomre 1981), a much stronger tidal field would be required to produce a pronounced two-arm distortion. However, the velocity map in the inner parts (Kam *et al.* 2015) seems too regular to be consistent with the strong tidal perturbation a low-mass disk would require.

6. CONCLUSIONS

We have demonstrated, for model galaxies lacking a dense center, that a disk embedded in a live, *i.e.* responsive, halo tends to form a strong bar. This is true, even when the disk is sufficiently sub-maximal that it is expected to be stable by the traditional stability criteria (Ostriker & Peebles 1973; Efstathiou, Lake & Negroponte 1982). It is important to realize that this instability is one of the combined disk and halo system; therefore, stability studies of disks embedded in rigid halos do not tell the full story, and stability criteria derived from them do not apply to galaxies having live halos.

We have found that none of the unstable modes presented in this work has an ILR, and that the mechanism for the linear mode remains that of feedback through the center, as outlined by Toomre (1981). However, his picture of swing amplification at corotation cannot be the whole story, since the work reported here demonstrates that angular momentum loss to the halo is another source of wave amplification. In other work (Berrier & Sellwood 2016), we find that linear bar instabilities are absent in models with dense bulges that inhibit wave reflection off the center.

The vigor of the disk instability in a live halo is strongly related to the ability of disk density variations to couple to near circular orbits in the halo. Therefore, compared

with an isotropic halo of a given mass, higher growth rates are found when the halo DF is tangentially biased, and lower when it is radially biased. Note that in all cases presented here, the halo has no net rotation. Increasing the halo mass slows the instability, but slowly growing modes persist even in very strongly submaximal disks embedded in isotropic halos.

The bars formed in these simulations are very strong, but their lengths are consistent with those observed in real galaxies. Gadotti (2011) finds the median value $a_B/R_d \simeq 1.5 \pm 0.5$, where a_B is the bar semi-major axis. Note that the value of R_d he used was that in the galaxy he observed, *i.e.*, after the bar formed. We find $a_B/R_{d,\text{new}} \simeq 1.5$ in our models, since the scale length of the disk outside the bar is about twice that of the original disk. The abruptly truncated halos of the models used here prevented further growth of the bars, of the kind reported by Athanassoula & Misiriotis (2002) and by Martinez-Valpuesta, Shlosman & Heller (2006), which would make them unrealistically long and strong (*cf.* Erwin 2005). Such bars would be unmistakable in any well resolved galaxy image, and their absence in galaxies with gently rising rotation curves presents a major unsolved puzzle.

Galaxy dynamics has turned out to be much richer and more complex than anyone imagined. The fact that a surprise such as that presented here could turn up after almost a half-century of simulations should remind us of how much more we have to learn, and how much may lie buried in the confusing behavior of simulations that attempt to include everything that could be important.

I wish to thank Joel Berrier for his persistent reports of bars in simulations with live halos that prompted this study. His help, both with discussions and for researching the topic of anisotropy in halos from structure formation simulations, is gratefully acknowledged. The comments of an anonymous referee helped to clarify several points. This work was supported by NSF grants AST/1108977 and AST/1211793.

REFERENCES

- Athanassoula, E., Bosma, A. & Papaioannou, S. 1987, *A&A*, **179**, 23
- Athanassoula, E. & Misiriotis, A. 2002, *MNRAS*, **330**, 35
- Athanassoula, E. & Sellwood, J. A. 1986, *MNRAS*, **221**, 213
- Berrier, J. C. & Sellwood, J. A. 2016, *ApJ*, (in preparation)
- Binney, J. & Tremaine, S. 2008, *Galactic Dynamics* (2nd ed.; Princeton: Princeton University Press)
- Carignan, C. & Freeman, K. C. 1985, *ApJ*, **294**, 494
- Catinella, B., Giovanelli, R. & Haynes, M. P. 2006, *ApJ*, **640**, 751
- Christensen, C. R., Governato, F., Quinn, T., *et al.* 2014, *MNRAS*, **440**, 2843
- Christodoulou, D. M., Shlosman, I. & Tohline, J. E. 1995, *ApJ*, **443**, 551
- Davis, B. L., Berrier, J. C., Shields, D. W., *et al.* 2012, *ApJS*, **199**, 33
- Debattista, V. P. & Sellwood, J. A. 2000, *ApJ*, **543**, 704
- de Blok, W. J. G., Walter, F., Brinks, E., Trachternach, C., Oh, S.-H. & Kennicutt, R. C., Jr. 2008, *AJ*, **136**, 2648
- Dejonghe, H. 1987, *MNRAS*, **224**, 13
- Diemand, J. & Moore, B. 2011, *ASL* **4**, 297
- D’Onghia, E., Vogelsberger, M. & Hernquist, L. 2013, *ApJ*, **766**, 34
- Efstathiou, G., Lake, G. & Negroponte, J. 1982, *MNRAS*, **199**, 1069
- Elmegreen, B. 1996, in *IAU Colloq.* **157**, *Barred Galaxies*, ed. R. Buta, D. A. Crocker & B. G. Elmegreen (San Francisco: ASP Conf series **91**), 197
- Erwin, P. 2005, *MNRAS*, **364**, 283
- Evans, N. W. & Read, J. C. A. 1998, *MNRAS*, **300**, 106
- Fujii, M. S., Baba, J., Saitoh, T. R., Makino, J., Kokubo, E. & Wada, K. 2011, *ApJ*, **730**, 109
- Gadotti, A. D. 2011, *MNRAS*, **415**, 3308
- Goldreich, P. & Lynden-Bell, D. 1965, *MNRAS*, **130**, 125
- Grand, R. J. J., Kawata, D. & Cropper, M. 2012, *MNRAS*, **426**, 167
- Governato, F., Brook, C., Mayer, L., *et al.* 2010, *Nature*, **463**, 203
- Hohl, F. 1971, *ApJ*, **168**, 343
- Jalali, M. A. 2007, *ApJ*, **669**, 218
- Julian, W. H. & Toomre, A. 1966, *ApJ*, **146**, 810
- Kalnajs, A. J. 1972, *ApJ*, **175**, 63
- Kalnajs, A. J. 1977, *ApJ*, **212**, 637
- Kam, Z. S., Carignan, C., Chemin, L., Amram, P. & Epinat, B. 2015, *MNRAS*, **449**, 4048
- Lynden-Bell, D. & Kalnajs, A. J. 1972, *MNRAS*, **157**, 1
- Mark, J. W.-K. 1974, *ApJ*, **193**, 539
- Martinez-Valpuesta, I., Shlosman, I. & Heller, C. 2006, *ApJ*, **637**, 214
- Miller, R. H., Prendergast, K. H. & Quirk, W. J. 1970, *ApJ*, **161**, 903

- Monaghan, J. J. 1992, *ARAA*, **30**, 543
- Ostriker, J. P. & Peebles, P. J. E. 1973, *ApJ*, **186**, 467
- Regan, M. W. & Vogel, S. N. 1994, *ApJ*, **434**, 536
- Sackett, P. D. 1997, *ApJ*, **483**, 103
- Sánchez-Janssen, R., Méndez-Abreu, J. & Aguerri, J. A. L. 2010
MNRAS, 406, L65
- Scannapieco, C., Wadepuhl, M., Parry, O. H., *et al.* 2012,
*MNRAS***423**, 1726
- Sellwood, J. A. 1989, *MNRAS*, **238**, 115
- Sellwood, J. A. 2003, *ApJ*, **587**, 638
- Sellwood, J. A. 2013, in *Planets Stars and Stellar Systems*, v.5,
eds. T. Oswalt & G. Gilmore (Heidelberg: Springer) p. 923
(arXiv:1006.4855)
- Sellwood, J. A. 2014, arXiv:1406.6606 (on-line manual:
<http://www.physics.rutgers.edu/~sellwood/manual.pdf>)
- Sellwood, J. A. & Athanassoula, E. 1986, *MNRAS*, **221**, 195
- Sellwood, J. A. & Carlberg, R. G. 1984, *ApJ*, **282**, 61
- Sellwood, J. A. & Evans, N. W. 2001, *ApJ*, **546**, 176
- Sellwood, J. A. & McGaugh, S. S. 2005, *ApJ*, **634**, 70
- Sellwood, J. A. & Moore, E. M. 1999, *ApJ*, **510**, 125
- Toomre, A. 1981, in *The Structure and Evolution of Normal Galaxies*, ed. S. M. Fall & D. Lynden-Bell (Cambridge: Cambridge University Press), p. 111
- Weinberg, M. D. 1985, *MNRAS*, **213**, 451
- Young, P. 1980, *ApJ*, **242**, 1232
- Zang, T. A. 1976, *PhD thesis*, MIT